

# Finite-Element Modeling of Hybrid Concrete-Masonry Frames Subjected to In-Plane Loads

Laura Redmond, Ph.D.<sup>1</sup>; Andreas Stavridis, A.M.ASCE<sup>2</sup>; Lawrence Kahn, F.ASCE<sup>3</sup>; and Reginald DesRoches, F.ASCE<sup>4</sup>

**Abstract:** Caribbean-style hybrid concrete-masonry structures consist of a RC frame infilled with partially grouted and reinforced masonry walls that are connected to the RC frame with cast-in-place dowels along one or more edges of the infill. Currently, there is little guidance in existing codes for the assessment of infills with such connections to the bounding frame. This paper proposes a finite-element modeling scheme for hybrid concrete-masonry structures combining smeared crack and interface elements. The model is used to predict the behavior of two hybrid concrete-masonry frames subjected to cyclic loading. The proposed finite-element modeling scheme closely predicts the peak capacity, the displacement at peak capacity, and the damage patterns of the test structures. Finally, sensitivity studies are conducted with the validated numerical models to investigate the influence of the dowel connections and masonry properties on the seismic performance of these structures. The results indicate that increasing the amount of reinforcement in the masonry infill makes the influence of the dowel connections become more pronounced, increases the strength of the structure, and lowers its ductility. DOI: 10.1061/(ASCE)ST.1943-541X.0001913. © 2017 American Society of Civil Engineers.

**Author keywords:** Analysis and computation; Masonry; Finite element method; Lateral loading.

## Introduction

Hybrid concrete-masonry structures in the Caribbean typically consist of a RC frame with partially grouted and reinforced infilled masonry walls. To improve the shear transfer between the frame and the infill and increase the out-of-plane resistance of the masonry, the infills are connected to the RC frame with cast-in-place dowel reinforcement along one or more edges of the frame-infill interface.

Simulating the seismic performance of this type of construction presents challenges for practicing engineers and researchers. The most reliable of the methods proposed is the finite-element (FE) method. The most challenging aspect of modeling concrete and masonry structures using finite elements is capturing their brittle behavior in tension and shear. One method to capture this material behavior is the embedded crack approach, which permits the opening of cracks in the mesh (e.g., Ngo and Scordelis 1967; Nilson 1968; Blaauwendraad and Grootenboer 1981; Hillerborg 1984). The advantage of discrete formulations is that the stresses at the free surface on either side of the crack reduce to zero. However, the formulation can be computationally expensive. A second method to capture cracking is to introduce interface elements at the locations

of possible cracks (e.g., Ali and Page 1988; Lotfi and Shing 1994; Lourenco 1996; Sayed-Ahmed and Shrive 1996; Minaie 2009), which may not be known a priori. A third method is the smeared crack approach, which represents cracking by a change in the element stiffness with either fixed or rotating crack formulations (e.g., Rashid 1968; Suidan and Schnobrich 1973; Bazant and Cedolin 1979).

This paper proposes a modeling scheme for hybrid concrete-masonry that combines the discrete and fixed smeared crack approaches with discrete truss reinforcement. The study expands the modeling scheme of Stavridis and Shing (2010) for unreinforced masonry infill using the element formulations of Lotfi and Shing (1994), and introduces a new meshing scheme for partially grouted masonry reinforcement and a methodology to account for the dowel action of the masonry reinforcement across the masonry bed joints. The proposed modeling scheme is used to predict the behavior of two full-scale hybrid concrete-masonry test specimens (Redmond et al. 2016b), where Frame 1 has dowel connections on all edges of the infill and Frame 2 has dowel connections only at the base of the infill. The finite-element models can predict the peak strength of the test frames within 10% of the actual strength and capture the main features of the failure patterns. Finally, sensitivity studies are conducted with the analytical models to understand the influence of the dowel connections and masonry properties on the performance of the hybrid concrete-masonry frames. The results indicate that increasing the amount of reinforcement in the masonry infill makes the influence of the dowel connections become more pronounced, increases the strength of the structure, and lowers the ductility of the structure.

## Description of Test Specimens

Two hybrid concrete-masonry test specimens were tested in the Georgia Institute of Technology Structural Engineering and Materials Laboratory (Redmond et al. 2016b). These structures consisted of a RC frame with partially grouted and reinforced infill

<sup>1</sup>Structural Engineer, School of Civil and Environmental Engineering, Georgia Institute of Technology, 790 Atlantic Dr., Atlanta, GA 30332 (corresponding author). ORCID: <https://orcid.org/0000-0001-5125-7656>. E-mail: [laura.redmond@gatech.edu](mailto:laura.redmond@gatech.edu)

<sup>2</sup>Professor, Dept. of Civil, Structural and Environmental Engineering, Univ. of Buffalo, Buffalo, NY 14260.

<sup>3</sup>Professor, School of Civil and Environmental Engineering, Georgia Institute of Technology, 790 Atlantic Dr., Atlanta, GA 30332.

<sup>4</sup>Professor, School of Civil and Environmental Engineering, Georgia Institute of Technology, 790 Atlantic Dr., Atlanta, GA 30332.

Note. This manuscript was submitted on June 25, 2016; approved on June 12, 2017; published online on November 8, 2017. Discussion period open until April 8, 2018; separate discussions must be submitted for individual papers. This paper is part of the *Journal of Structural Engineering*, © ASCE, ISSN 0733-9445.

masonry walls and connections to the RC frame. The test frame was extracted from the bottom story of a 5-story office building designed according to the 2009 International Building Code (ICC 2009) for the highest level of seismic hazard in Trinidad (spectral acceleration of  $1.73g$  at  $0.2$  s for a return period of 2,475 years). The RC frame was designed as a special moment frame according to ACI 318-14 (ACI 2014) ( $R = 8.0$  from ASCE 7-10), carrying all of the gravity and lateral loads. The weight of the masonry infill was accounted for with a line load of  $7.3$  kN/m ( $500$  lb/ft), but its stiffness was neglected. The infill panels of the experimental frames were constructed using  $203 \times 203 \times 406$  mm ( $8 \times 8 \times 16$  in.) hollow concrete masonry units (CMUs) and a 3:1 sand–portland cement mortar mix. The horizontal reinforcement within the masonry wall consisted of a single 10-mm (#3) reinforcing bar placed in the bed joint along the centerline of the CMU, spaced vertically every 610 mm (24 in.). The vertical reinforcement was a 16-mm (#5) reinforcing bar spaced every 813 mm (32 in.).

The reinforcing details for Frame 1 are shown in Fig. 1; Frame 2 was identical except that connections were only present between the foundation and the base of the masonry infill.

## Modeling Scheme

The modeling scheme adopted here for hybrid concrete-masonry structures uses the smeared crack elements and the double-noded, zero-thickness interface elements developed by Lotfi and Shing (1991). The smeared crack element uses a von Mises yield criterion combined with a tension cutoff criterion as shown in Fig. 2(a). When the latter is reached, the element adopts an orthotropic law with fixed axes of orthotropy parallel and perpendicular to the directions of the principal stresses. The interface element is elastic in compression and simulates the Mode I, Mode II, and mixed-mode fracture using a plasticity-based formulation with a hyperbolic

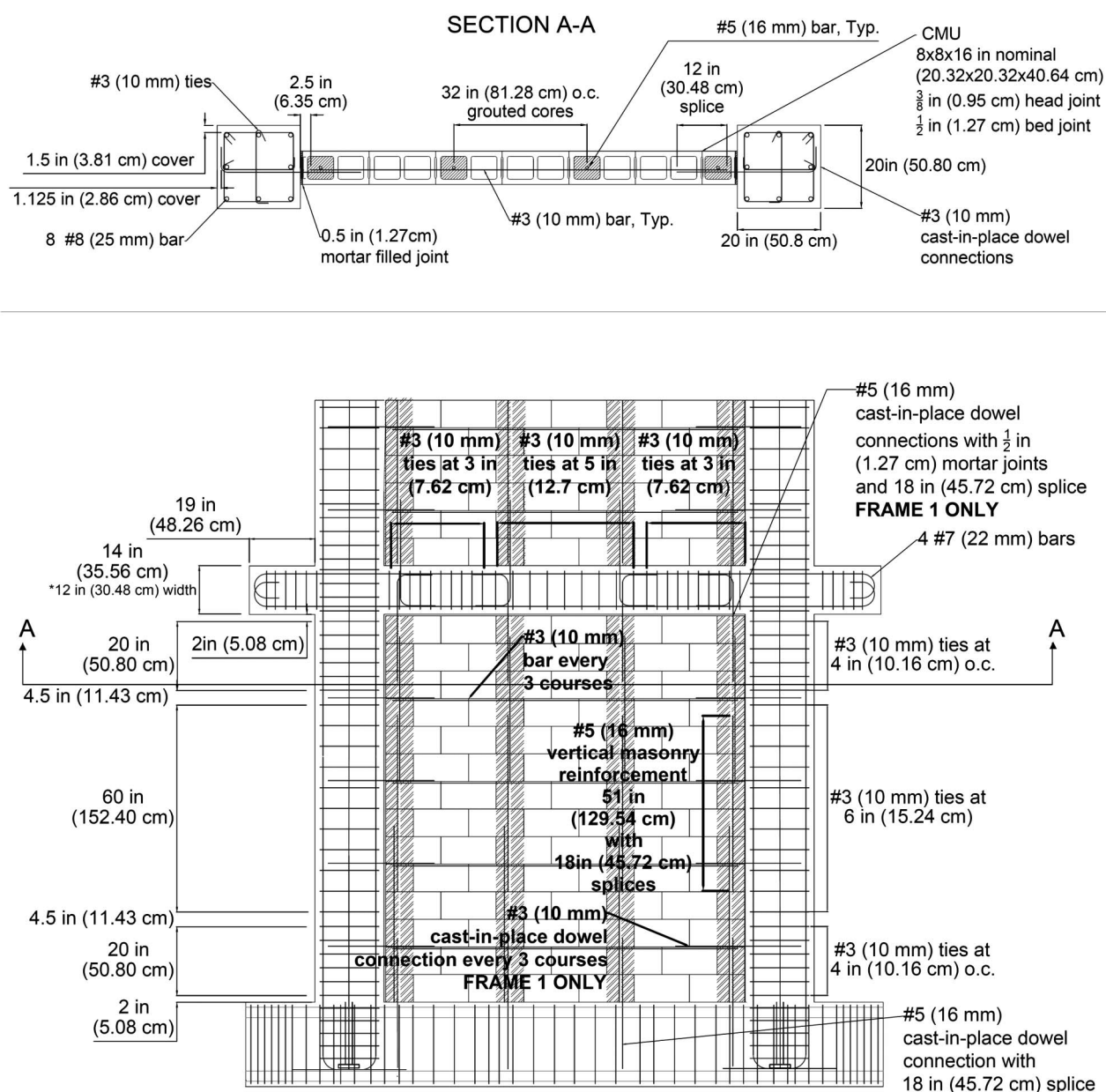
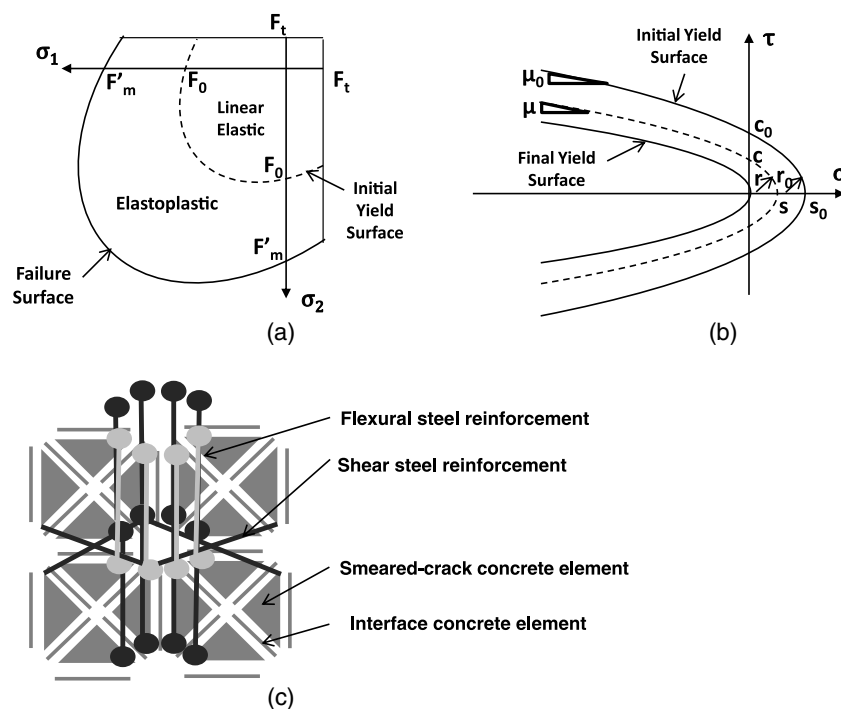


Fig. 1. Design details of specimen Frame 1



**Fig. 2.** Material behavior of elements developed by Lotfi and Shing (1994): (a) smeared crack element yield and failure surface; (b) interface element yield surface; (c) concrete modeling scheme developed by Stavridis and Shing (2010)

yield surface, which is a smooth transition between the Mohr–Coulomb criterion and a tension cutoff, as illustrated in Fig. 2(b). This element is selected because it uses a nonassociate flow rule to scale the dilatancy. The reinforced concrete members are modeled using the scheme proposed by Stavridis and Shing (2010) and shown in Fig. 2(c). The concrete model includes a module consisting of four triangular smeared crack elements connected by interface elements at an angle close to  $\pm 45^\circ$  to capture shear cracking. The modules are connected with interface elements at 0 and  $90^\circ$ , which are crossed by elastic-perfectly plastic truss elements representing the shear and flexural reinforcement. The truss elements are connected to the corners of the smeared crack elements to provide numerical stability, but also to ensure that each potential crack in a RC element is resisted by the realistic amount of reinforcement. In this study, a modeling methodology for partially grouted reinforced masonry infill considering the dowel action of masonry reinforcement is proposed.

### Partially Grouted Reinforced Masonry

The proposed modeling scheme for partially grouted reinforced masonry is shown in Fig. 3. The single lines in the figure represent the double-noded, zero-thickness interface elements. This modeling scheme uses more elements than previous formulations (Stavridis and Shing 2010; Sayah et al. 2013); however, the proposed module of eight smeared crack elements used to represent the grouted cells permits the development of shear and vertical cracks as has been observed in tests of partially grouted masonry walls subjected to in-plane lateral loads (Minaie 2009). The cells of the ungrouted CMUs are modeled with two smeared crack elements without using diagonal interface elements. This scheme is selected for computational efficiency because shear failure of these units is not anticipated because crushing is expected to be the dominant failure mode of the hollow units. Both the ungrouted and the grouted cells are connected to one another via interface elements representing the webs of the

CMUs, as well as the bed joints and the head joints. The interface elements for the bed joints between grouted cells are referred to as grouted bed joints and represent the mortar and the grout within the bed joint. The interface elements for the bed joints between ungrouted cells are referred to as ungrouted bed joints and represent only the mortar connecting the CMUs. The thicknesses of the ungrouted mortar bed joints and head joints are set equal to the average thickness of the mortar joints along the length or the height of the CMU, respectively.

The scheme used to model the reinforcement is shown in Fig. 4. Each vertical reinforcing bar is modeled with eight truss elements at the center of the grouted cell so that every smeared crack element in the reinforced and grouted cells is connected to a truss element representing the vertical reinforcement (Sayah et al. 2013). In hybrid concrete-masonry structures in the Caribbean, the horizontal reinforcement is only bonded to the grouted cells. Hence, the horizontal reinforcement is not connected to the ungrouted cells, as shown in Fig. 4(a). The proposed modeling scheme can be adapted to account for a variety of masonry construction details including continuously bonded bed joint reinforcement or bond beams, as shown in Figs. 4(b and c), respectively.

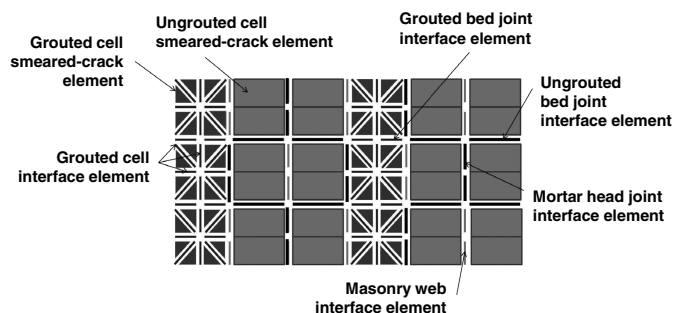


**Fig. 3.** Schematic for partially grouted reinforced masonry



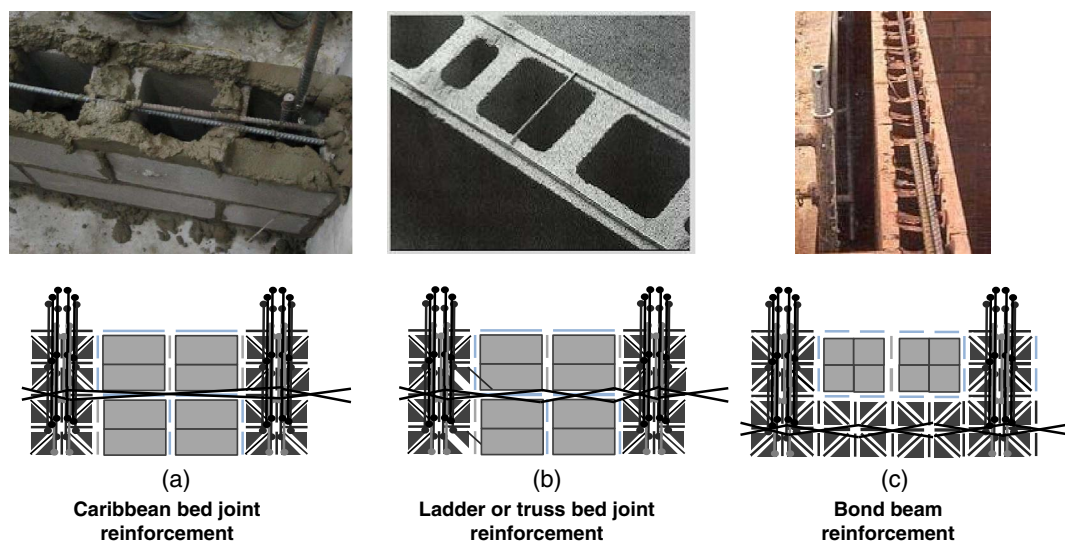


**Fig. 4.** Connectivity of truss elements for different horizontal reinforcement schemes: (a) Caribbean bed joint reinforcement (image by Laura Redmond); (b) ladder or truss bed joint reinforcement; (c) bond beam reinforcement [(b and c) images courtesy of The Masonry Society and its Members]

### Dowel Action of Reinforcement

In some cases of hybrid concrete masonry, cast-in-place reinforcing bars are used to connect the masonry infill to the RC columns and beams above and below the infill. These dowel bars have 90° bends and are anchored to the far face of the RC beams or RC columns, or at a minimum 457 mm (18 in.) embedment in the foundation, as shown in Fig. 1. These bars are placed within the masonry bed joints or the grouted cells, and provide resistance primarily through the dowel action. The truss elements used to model reinforcement cannot transfer shear forces due to the pinned end conditions. In order to represent the shear resistance of the dowel bars, additional elastic-perfectly plastic truss elements are placed in a zigzag pattern between the elements representing the masonry infill and the elements representing the concrete columns. This approach was first used to simulate a 3-story 3-bay RC frame with hollow clay tile infills and externally applied mesh-reinforced mortar (Redmond et al. 2016a). That study indicates that the proposed modeling technique adequately simulates the behavior of the physical specimen using two horizontal bars with a total area equal to 25% of the cross-sectional area of the dowel bar to represent the shear contribution of the bar to the interface. The parametric study considers bar areas up to 100% of the physical bar area. The results indicate that the model is not sensitive to changes in the area of these bars beyond 25% of the physical dowel bar area.

A similar approach is used in this study to simulate the dowel action of vertical reinforcement across the grouted bed joints. As shown in Fig. 5, truss elements are added within the bed joints to simulate the shear resistance of the flexural reinforcement. The area of these additional truss elements can be estimated based on the values proposed to simulate the dowel action of rebar in concrete, which range from 25 to 50% of the physical bar area (Dulacska 1972; Soroushian et al. 1986; Paulay et al. 1974). This modeling approach allows a realistic representation of shear failure because an interface element simulating the bed joint reaches its peak shear resistance and then softens before a truss element representing the dowel yields. Most existing models for reinforced masonry use the macromodeling method, which cannot capture local behavior of the bed joints (Colotti 2001; Wu et al. 2016). Previously proposed micromodeling schemes did not consider the contribution of flexural reinforcement to the shear capacity of the bed joint

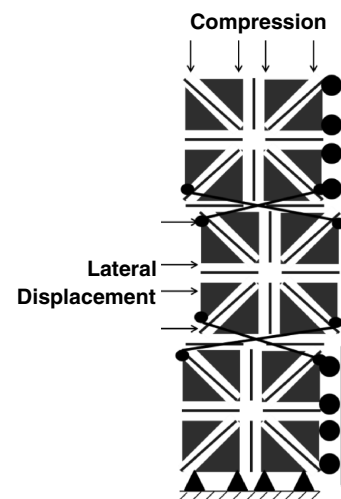


**Fig. 5.** Truss elements placed along the bed joints to represent the shear resistance of the flexural reinforcement

(Stavridis and Shing 2010; Sayah et al. 2013). This effect becomes more significant in reinforced masonry with weak mortar or grout.

The truss elements used to model the dowel action of the vertical reinforcement also increase the capacity of the masonry in tension and bending. The influence of these truss elements on tension and bending capacity is examined in a parametric study considering prisms with weak and strong grout subjected to pure tension and three-point bending with effective dowel reinforcement ratios of 25–50%. In all cases, the prism tensile strength increases less than 0.5%, while the flexural resistance increases between 6 and 22%. In order to minimize the influence on the flexural resistance, 25% effective dowel area is used in the proposed model.

### Material Calibration

The proposed finite-element modeling scheme is used to predict the behavior of the two full-scale hybrid concrete-masonry structures tested in the Structural Engineering and Materials Laboratory at

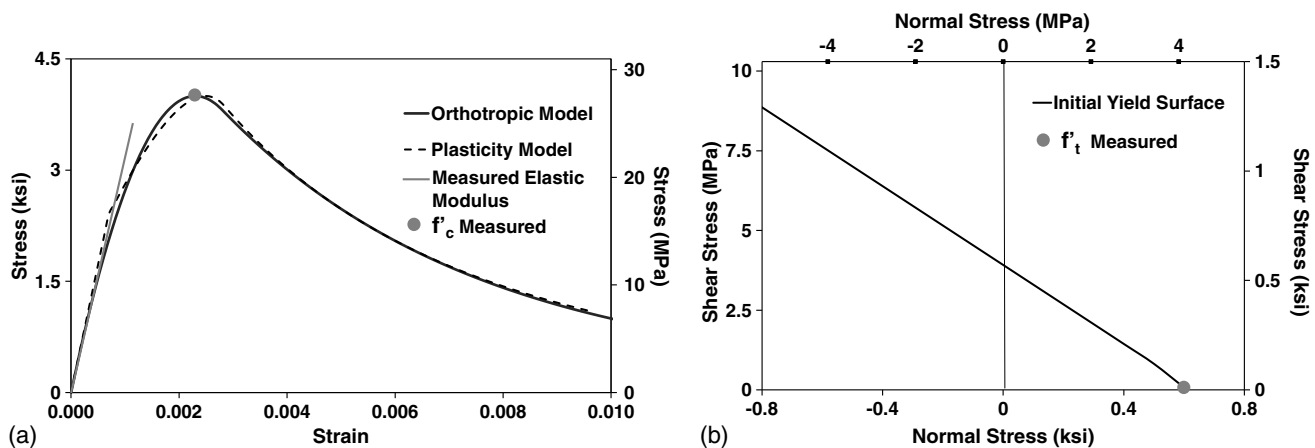


**Fig. 6.** Calibrated material curves for concrete compression and shear behavior: (a) smeared crack element compressive stress versus strain; (b) interface element shear stress versus normal stress

Georgia Institute of Technology (Redmond et al. 2016b). The models are calibrated using data from materials tests conducted prior to the experiments.

The stiffness and compressive strength are calibrated with results from compression tests, while cylinder tests of  $152 \times 305$  mm ( $6 \times 12$  in.) concrete cylinders [ASTM C469 (ASTM 2013d)] are used to obtain the tensile strength of concrete following the procedure from Stavridis and Shing (2010). The fracture energy is assumed to be proportional to the compressive strength of the concrete and it is taken from data available in the literature (Hillerborg 1983). The initial and residual slope of yield surface for the interface elements  $\mu_0$  and  $\mu_r$  and the initial and residual radii of the yield surface for the interface elements  $r_0$  and  $r_r$  are taken from Mehrabi et al. (1994). In Fig. 6(a), the compressive stress-strain curve for both the plasticity model used to describe the material behavior before cracking and the orthotropic model used to describe the behavior of the cracked materials is calibrated to the elastic modulus and compressive strength obtained from the material tests. The postpeak behavior is approximated using data from the literature. In Fig. 6(b), the calibrated curve for the interaction of the normal and shear stresses is presented along with the tensile strength, determined by split tension tests. The slope of the shear-normal stress is taken from Mehrabi et al. (1994).

The prism strength of the ungrouted masonry is obtained from compression tests of two-unit prisms [ASTM C1314 (ASTM 2013a)]. The elastic modulus was determined by recordings of dial gauges mounted across the bed joint during the test. The compressive behavior of the ungrouted masonry is modeled using the data from prism tests and the calibration methodology of Stavridis and Shing (2010) and it is shown in Fig. 7(a). The tensile strength of the ungrouted masonry units is approximated as 10% of the unit's compressive strength and the fracture energy of the ungrouted masonry unit is determined using values from Stavridis and Shing (2010). The values of  $\mu_0$ ,  $\mu_r$ ,  $r_0$ , and  $r_r$ , which govern the shear behavior of the interface elements simulating the ungrouted bed joints, are taken from Mehrabi et al. (1994).

The calibrated compression behavior of the grouted cells is based on prism tests and it is shown in Fig. 7(b). The tensile strength of the grouted masonry unit is approximated as 10% of the grout compressive strength, determined from tests of grout cubes prepared according to ASTM C1019 (ASTM 2013c). The fracture energy of the grouted masonry units is assumed to be proportional to the compressive strength of the grout and interpolated from values in the literature (Hillerborg 1983). The values of  $\mu_0$ ,  $\mu_r$ ,  $r_0$ , and

$r_r$  used in Mehrabi et al. (1994) for concrete are used in this study for the grout in the absence of more appropriate data.

Triplet tests conducted under different levels of normal stress are used to calibrate the normal stress versus shear stress relation of the interface element for the ungrouted and grouted bed joints [DIN EN1052-3 (DIN 2007)], while the tensile strength of the ungrouted and grouted bed joints is obtained from bond wrench tests [ASTM C1072 (ASTM 2013b)]. The calibrated material relations for masonry bed joint shear behavior are shown in Figs. 7(c and d). The bond strength of the head joints is selected to be 50% of the bed joint strength because head joints often have lower bond strength compared with the bed joints (Drysdale et al. 1994; NCMA 2004). The discrete crack elements along the column-infill interfaces are assigned the same properties as the head joints, while the beam-infill interfaces are assigned the same properties as the bed joints.

## Comparison of Numerical and Experimental Results

The peak lateral force and displacement at peak lateral force for the two experimental frames match well with the predictions from the FE models, as shown in Figs. 8(a and b). The predicted peak force and corresponding displacement for Frame 1 are within 2% of their experimental counterparts. The model correctly predicts the capacity of Frame 2 to be less than that of Frame 1, but it underestimates the capacity of Frame 2 by 9.6% and does not capture the strength degradation as closely. The initial stiffness of both FE models is also greater than the stiffness observed experimentally. This is expected because physical specimens have additional flexibility due to construction and support imperfections that are not accounted for in the numerical models. Compared with the physically tested frames, the FE models show less brittle postpeak behavior. In lieu of the proposed calibration method, the degradation of the concrete and masonry element material curves in the postpeak regime can be calibrated to subassembly tests that characterize hysteretic behavior. However, the proposed model has the advantage of utilizing common subassembly tests for calibration and is able to capture the peak capacity, the displacement at peak capacity, and the failure modes of the tested hybrid concrete-masonry structures.

In terms of the failure mechanism, the cracking patterns are similar, although damage initiates in both FE models at lower drift levels compared with the experiments. The lateral drift used in this study is defined as the ratio between the lateral displacement at the middle of the beam to the height measured from the top of the

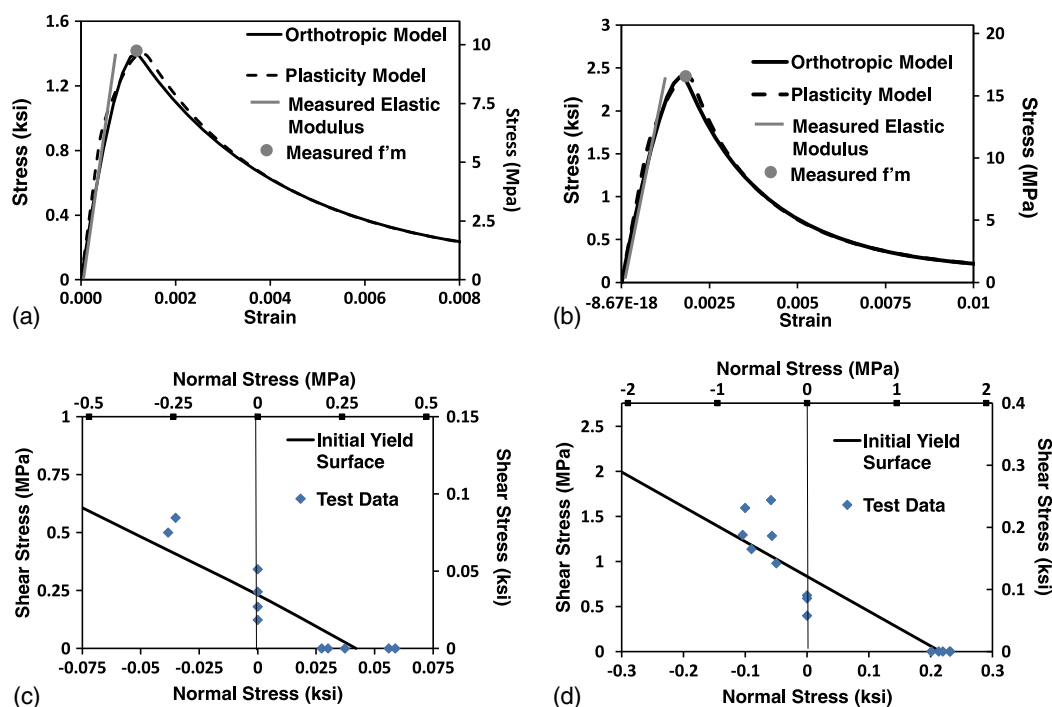


**Fig. 7.** Calibrated material laws for masonry compression and bed joint shear behavior: (a) ungrouted prism compressive stress versus strain; (b) grouted prism compressive stress versus strain; (c) ungrouted bed joint shear stress versus normal stress; (d) grouted bed joint shear stress versus normal stress

foundation to the middle of the beam. At drift levels of less than 0.083% [2.5 mm (0.1 in.)], the test measurements are significantly influenced by compliances due to the test fixture and construction imperfections, such as gaps between the infill and RC frame. For the cracking patterns observed at very low drift levels, the FE models predict the initial cracking along the RC column-infill interface followed by the RC beam-infill interface. Slip gauges on the test specimens indicated the RC beam-infill interface cracked first, followed by the RC column-infill interface. Bed joint cracking propagated throughout the infill in both FE models by 0.017% drift [0.51 mm (0.02 in.)]. In the test structures, cracking of the masonry infill was not observed until considerably larger drift levels. Bed joint cracking was observed in experimental Frame 2 at 0.13% drift [3.81 mm (0.15 in.)]. In Frame 1, the first cracks were diagonal,

initiating at 0.25% drift [7.62 mm (0.30 in.)]. The cracking patterns of the physical and FE models at low displacement levels are shown in Fig. 9. For all images from the FE models presented in this paper, cracking is denoted by the white lines and crushing by the gray Xs. In the test structures, cracks opening in positive loading cycles are shown in black and cracks opening during negative loading cycle cracks are shown in white.

The next significant damage stage in the FE models is the development of flexural cracks in the windward column, in which tension is induced by the overturning moment, at 0.25% drift. These cracks initiate at the base of the windward column up to the height of the fifth course of the masonry infill, at the top of the windward column, and at the bottom of the leeward column, as shown in Figs. 10(a and b) for the two models. A difference

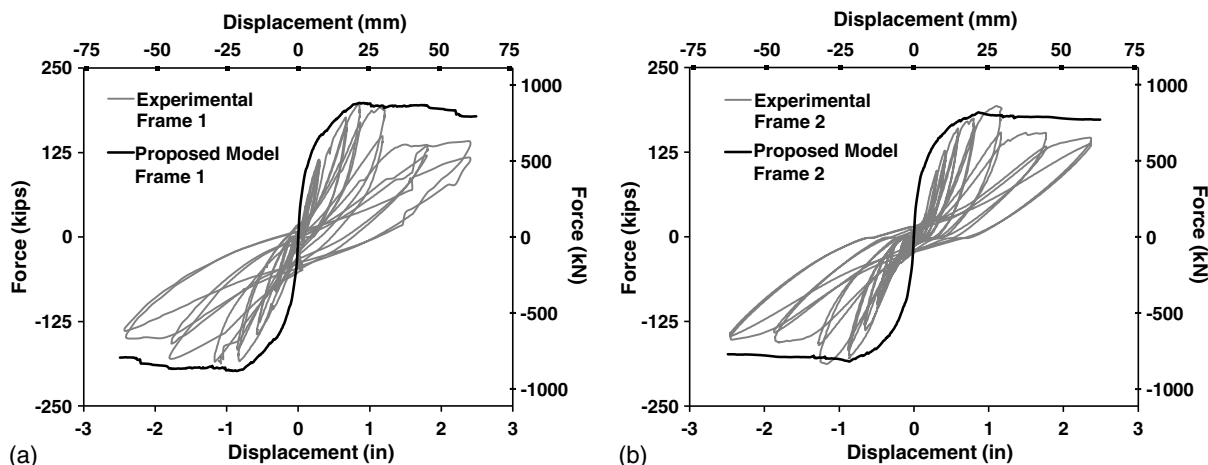


**Fig. 8.** Force-displacement plots of the experimental and analytical frames: (a) Frame 1 (full connection); (b) Frame 2 (connection only at base)

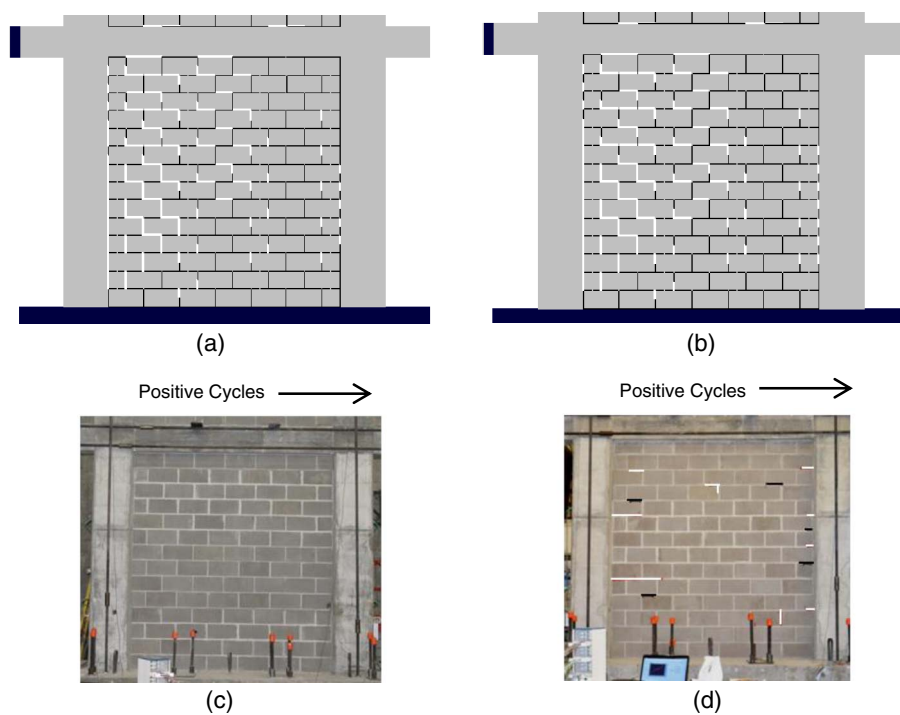


**Fig. 9.** Initial cracking patterns in the numerical models and the test specimens: (a) FE model for Frame 1 at 0.012% drift (full connection); (b) FE model for Frame 2 at 0.012% drift (connection only at base); (c) Frame 1 at 0.13% drift (full connection); (d) Frame 2 at 0.13% drift (connection only at base)

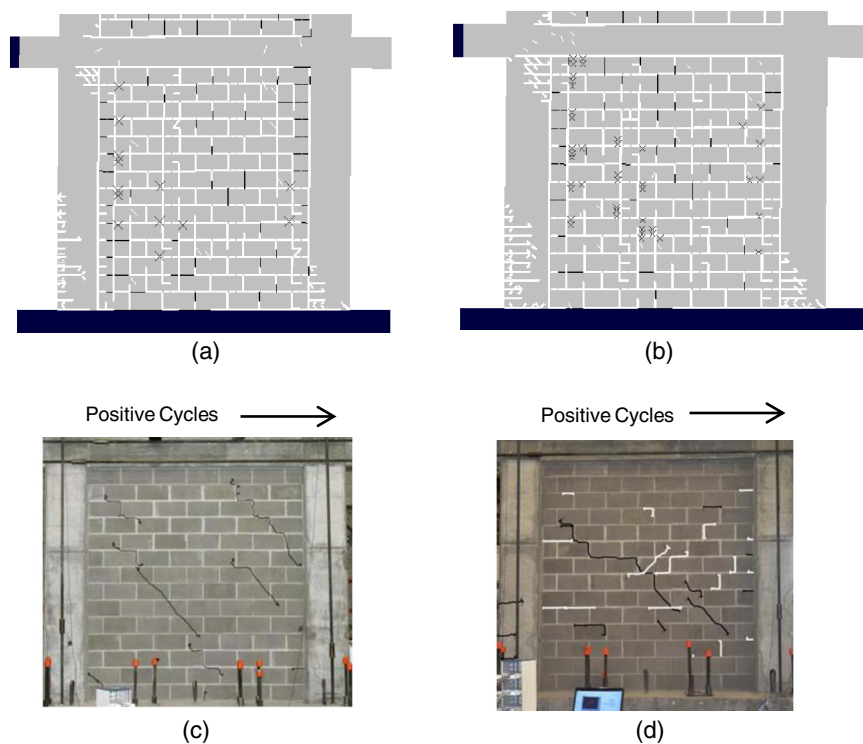


**Fig. 10.** Damage in the numerical models and the test specimen models at 0.25% drift: (a) FE model for Frame 1 at 0.25% drift (full connection); (b) FE model for Frame 2 at 0.25% drift (connection only at base); (c) Frame 1 at 0.25% drift (full connection); (d) Frame 2 at 0.25% drift (connection only at base)

between the two models is that the shear crack at the top of the windward column is larger in the FE model of Frame 2 than in that of Frame 1. Both FE models develop limited crushing throughout the masonry wall. The FE model accurately predicts the flexural

cracking in the windward column of Frame 2 at 0.25% drift, but no column cracks were observed in Frame 1 at this drift level, as shown in Figs. 10(d and c), respectively. Combined shear and flexural cracking at the interior face of the columns and masonry



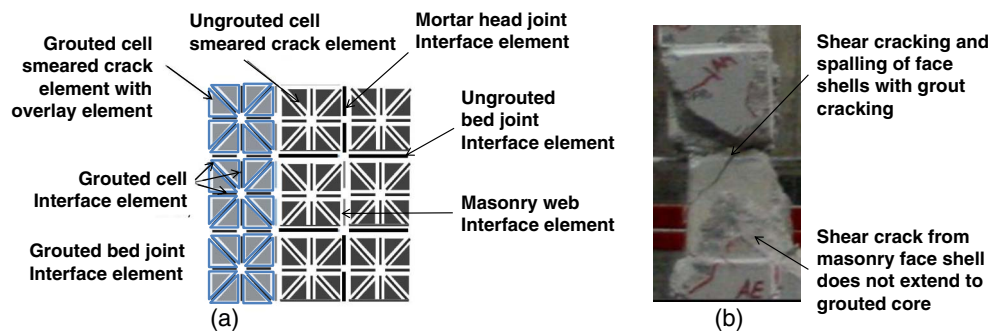


**Fig. 11.** (a) Alternative meshing scheme; (b) masonry cracking observed in the test

crushing consistent with the finite-element models were also observed in both test structures, but not until 0.35% drift. Diagonal cracking across the masonry face shells was observed in the tests. The corresponding FE models developed stair-stepped diagonal cracks along the bed joints and head joints, and only a few diagonal cracks in the smeared crack elements. This is due to a modeling scheme that does not include diagonal discrete crack elements in the modules representing the ungrouted cells for computational efficiency. This is a sufficient representation of the damage pattern and does not affect the results given the low load resistance of the ungrouted masonry units. One could include in the meshing scheme for the ungrouted masonry units diagonal interface elements to model these elements with the eight-element modules in a similar fashion as the grouted units.

Another modeling alternative to capture this failure pattern more realistically would be to use the same 8-element modules for all units incorporating the diagonal discrete crack elements, then add

a second layer of elements with shared nodes to simulate the effect of the grout in the case of grouted units, as shown in Fig. 11(a). This novel meshing scheme permits the face shells to crack even when the grouted cores do not, as observed in the tests [Fig. 11(b)]. The alternative mesh can more accurately capture cracking behavior, but at an increased computational cost.

In both FE models, the maximum strain in the column flexural reinforcement first exceeds the yield strain at the base of the columns. The test data, however, indicate that the reinforcement in the columns first yielded at approximately the elevation where the spliced dowels in the masonry wall terminated (Redmond et al. 2016b). A parametric study indicated that if the effective dowel bar area, shown in Fig. 5, and the flexural reinforcement area through the height of the dowel bars at the base of the masonry wall are doubled to account for the spliced dowel reinforcement, the location of initial yielding of the column flexural reinforcement moves up in elevation and corresponds to the test observations. At a drift of

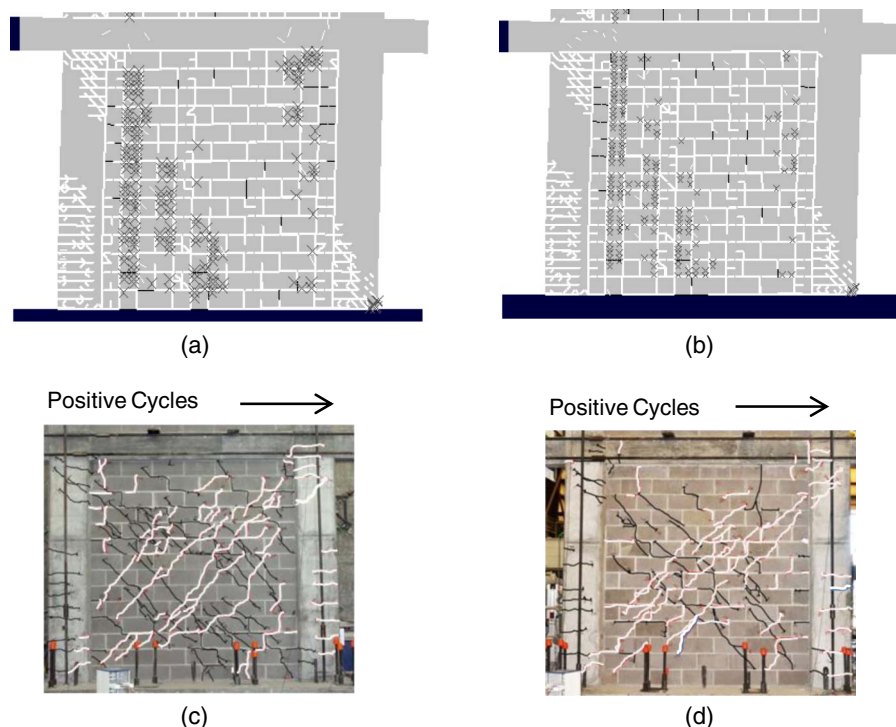


**Fig. 12.** Damage in the numerical models and the test specimens at 0.68% drift: (a) FE model for Frame 1 at 0.68% drift (full connection); (b) FE model for Frame 2 at 0.68% drift (connection only at base); (c) Frame 1 at 0.68% drift (full connection); (d) Frame 2 at 0.68% drift (connection only at base)



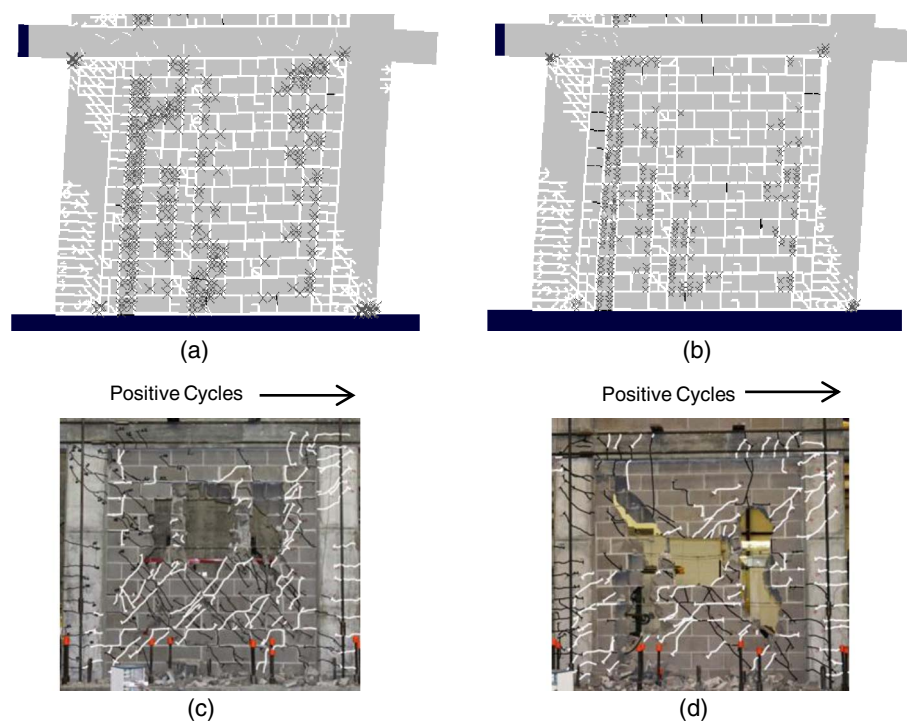


**Fig. 13.** Damage in the numerical models and test specimens at 2.0% drift: (a) FE model for Frame 1 at 2.0% drift (full connection); (b) FE model for Frame 2 at 2.0% drift (connection only at base); (c) Frame 1 at 2.0% drift (full connection); (d) Frame 2 at 2.0% drift (connection only at base)

0.68%, the cracking patterns in the test specimens are very similar to those predicted by the FE models as shown in Figs. 12(c and d).

By 2% drift, the FE models show significant crushing of the masonry, and more shear and flexural cracks develop in the columns, as shown in Figs. 13(a and b). Cracks also develop in the ends of the beams and in the beam-column joints. The Frame 2 FE model shows slightly more damage to the columns because the yielding of the column flexural reinforcement propagates higher than in the Frame 1 FE model. This matches well with the experimental results. By 2% drift, the ungrouted cells fell out from the masonry wall in both test structures. Significantly less masonry was lost in Frame 1, which had connections on all edges of the masonry wall. In both test structures, cracks formed at the ends of the beams and in the beam-column joints. The flexural cracks in the test frames continued to expand, but no additional shear cracks formed after the masonry began to fall out. By the end of the test at 2.0% drift, Frame 2 had slightly more damage to the RC columns and beam than Frame 1, and the infill was in danger of falling out of plane, as illustrated in Figs. 13(c and d).

### Influence of Dowel Connections and Masonry Properties

The validated numerical models are used to create two additional models to explore the influence of the dowel connections between the partially grouted infill wall and the bounding RC frame. The additional models have the same geometry and material properties as the experimental frames, but one model has no connections between the infill and the bounding RC frame, while the other has vertical connections from the infill to the foundation and the RC beam. The results are compared with the models of the test specimens in Table 1. The peak capacity of the numerical model of the frame with dowel connections to the RC frame at the top and bottom of the infill wall is within 1% of the capacity of the frame with

dowel connections on all edges of the masonry wall. The frame without any dowel connections has 2.5% less capacity than the frame with dowel connections only at the base of the wall. The frame with connections only at the top and the bottom of the infill shows the greatest ductility, reaching peak lateral capacity at 1.0% drift. Caribbean masonry units are substantially weaker than the CMUs used in the United States and the weakness of the masonry wall relative to the RC frame is likely the cause of the only subtle influence of the dowel connections.

The analytical models of Frames 1 and 2 are also used to study the influence of the masonry infill properties, which are varied, as shown in Table 2.

The parameters that show a significant influence on the peak capacity and displacement at peak capacity of the frames are vertical masonry reinforcement and dowel reinforcement spacing, vertical dowel reinforcement area, and prism strength of the ungrouted masonry. All other investigated parameters resulted in changes of less than 5%, or both the upper-value and the lower-value models increased the parameter of interest, or both the upper-value and the lower-value models decreased the parameter of interest. The results are shown in Figs. 14 and 15.

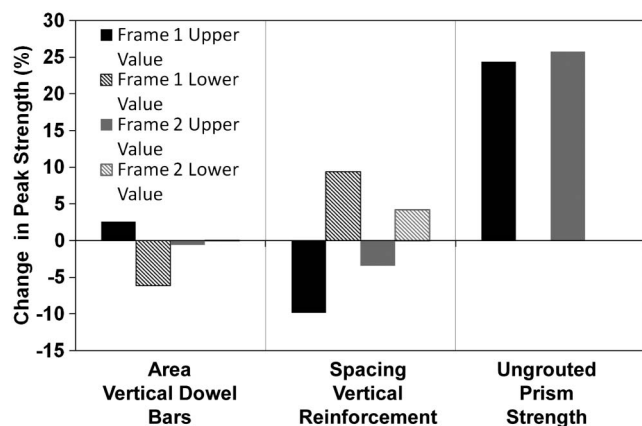
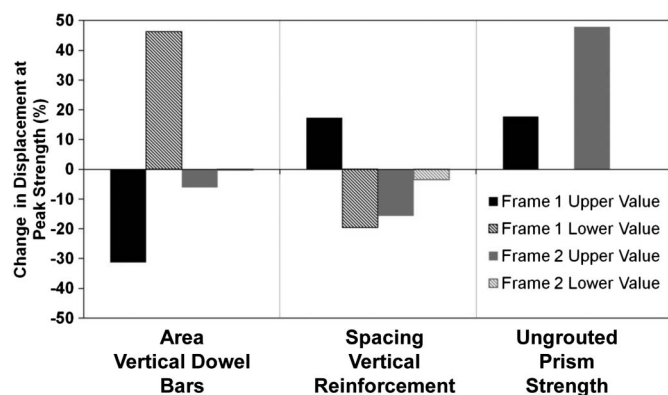
Although the dowel connections appeared to have only a subtle influence on the behavior of the modeled test specimens, decreasing the vertical reinforcement spacing (and dowel spacing)

**Table 1.** Performance of Analytical Hybrid Concrete-Masonry Frames with Various Dowel Connections

Dowel connections	Peak lateral capacity [kN (kip)]	Percentage drift at peak lateral capacity (%)
All edges	874.6 (196.6)	0.71
Beam to infill and foundation to infill	871.2 (195.9)	0.96
Foundation to infill	809.9 (182.1)	0.73
None	792.2 (178.1)	0.71

**Table 2.** Parameters for Sensitivity Study on Masonry Infill Properties

Parameter	Baseline quantity	Lower value	Upper value
UngROUTed prism strength	9.88 MPa (1.43 ksi)	N/A	19.31 MPa (2.8 ksi)
Grout compressive strength	21.03 MPa (3.0 ksi)	10.34 MPa (1.5 ksi)	41.37 MPa (6.0 ksi)
Mortar type	Type N	N/A	Type M
Horizontal masonry reinforcement area	10-mm (#3) bar	0.5 $\times$ nominal	2.0 $\times$ nominal
Vertical masonry reinforcement area	16-mm (#5) bar	0.5 $\times$ nominal	2.0 $\times$ nominal
Vertical dowel reinforcement area	16-mm (#5) bar	0.5 $\times$ nominal	2.0 $\times$ nominal
Horizontal dowel reinforcement area	10-mm (#3) bar	0.5 $\times$ nominal	2.0 $\times$ nominal
Vertical masonry reinforcement spacing	813 mm (32 in.)	406 mm (16 in.)	1,219 mm (48 in.)
Horizontal masonry reinforcement spacing	610 mm (24 in.)	406 mm (16 in.)	1,016 mm (40 in.)

**Fig. 14.** Influence of significant masonry infill properties on peak strength**Fig. 15.** Influence of significant masonry infill properties on displacement at peak strength

from 813 mm (32 in.) to 406 mm (16 in.) resulted in a more pronounced influence of the dowel connections. Frame 1, which had dowel connections on all edges of the masonry wall, showed an increase in peak capacity of 10% and a decrease in the displacement at peak capacity of 20%. Frame 2, which only had dowel connections at the base of the wall, showed an increase in peak capacity of only 4% and a decrease in the displacement at peak capacity of 4%. Reducing the area of the vertical dowel reinforcement by a factor of 2 resulted in a 6% reduction in the peak capacity of Frame 1 and a 46% increase in the displacement at peak strength. Frame 2 had only a 0.1% decrease in peak capacity and 0.4% decrease in displacement at peak strength. Increasing the prism strength of the ungrouted masonry by a factor of 2 resulted in an increase in peak strength of approximately 25% for both frames and an increase in

displacement at peak strength of 18% for Frame 1 and 47% for Frame 2.

In light of the results of the analytical studies, future work on this topic could include the experimental investigation of more densely reinforced masonry infills and stronger masonry units. In addition, investigations into a more balanced method of designing hybrid concrete-masonry structures such that the RC frame and the masonry wall can work more integrally may lead to a more effective and economical design.

## Conclusions

This study proposes a finite-element modeling scheme that can be consistently calibrated for hybrid concrete-masonry structures. The model combines the smeared crack and discrete crack approaches to model flexural and shear cracks, and uses truss elements to model the reinforcement. The proposed modeling scheme is unique because it is adaptable to partially and fully reinforced masonry and accounts for the contribution of the flexural reinforcement to the shear capacity of the bed joint via dowel action. As a result, the model accurately predicts the global failure mechanisms and local cracking patterns once it is calibrated using data from standard material tests. This modeling approach could be employed to investigate the local behavior and interaction along the interface between foundations and reinforced masonry walls, the local bed joint behavior in the reinforced masonry units, and/or the effects of different reinforcement schemes on the behavior of reinforced concrete frames with reinforced masonry infills.

The proposed methodology was applied to simulate the performance of two single-bay, single-story hybrid concrete-masonry frames. The models closely capture the peak strength, displacement at peak strength, and failure mechanisms of the two frames. The models were also used to conduct numerical studies on the influence of the dowel reinforcement and masonry material properties. The models show only a subtle influence of the dowel connections on the force-displacement behavior of the hybrid concrete-masonry frames. This is likely due to the lower strength of the masonry wall relative to the bounding RC frame. However, as the reinforcement quantity in the masonry infill is increased, the influence of the dowel connections becomes more pronounced. Gains in peak lateral force capacity can be obtained by increasing the size of the vertical dowel bars or decreasing the vertical reinforcement spacing. However, the increase in strength due to the higher reinforcement ratio comes at the cost of decreased ductility.

## Acknowledgments

This material study was supported by the National Science Foundation Graduate Research Fellowship under Grant 2011129510. Travel support to Trinidad, Belize, Jamaica, and Puerto Rico was

provided by the Speedwell Foundation under the Caribbean Hazard and Mitigation Program (CHAMP). Sponsors for the experimental tests include Simpson Strong Tie, United Forming, and Jolley Masonry. However, the opinions expressed in this paper are those of the authors and do not necessarily represent those of the sponsors.

## Notation

The following symbols are used in this paper:

- $f'_c$  = ultimate compressive stress;
- $f'_t$  = ultimate tensile stress;
- $r$  = radius of yield surface for interface element;
- $r_r$  = residual radius of yield surface for interface element;
- $r_0$  = initial radius of yield surface for interface element;
- $s$  = tensile strength of interface element;
- $s_0$  = initial tensile strength of interface element.
- $\mu_r$  = residual slope of yield surface for interface element;
- $\mu_0$  = initial slope of yield surface for interface element;
- $\sigma$  = normal stress; and
- $\tau$  = shear stress.

## References

- ACI (American Concrete Institute). (2014). "Building code requirements for structural concrete." *ACI 318-14*, Farmington Hills, MI.
- Ali, S., and Page, A. W. (1988). "Finite element model for masonry subjected to concentrated loads." *J. Struct. Eng.*, 10.1061/(ASCE)0733-9445(1988)114:8(1761), 1761–1784.
- ASTM. (2013a). "Standard test method for compressive strength of masonry prisms." *ASTM C1314*, West Conshohocken, PA.
- ASTM. (2013b). "Standard test method for measurement of masonry flexural bond strength." *ASTM C1072*, West Conshohocken, PA.
- ASTM. (2013c). "Standard test method for sampling and testing grout." *ASTM C1019*, West Conshohocken, PA.
- ASTM. (2013d). "Standard test method for static modulus of elasticity and Poisson's ratio of concrete in compression." *ASTM C469*, West Conshohocken, PA.
- Bazant, Z. P., and Cedolin, L. (1979). "Blunt crack band propagation in finite element analysis." *J. Eng. Mech. Div.*, 105(2), 297–315.
- Blaauwendraad, J., and Grootenboer, H. J. (1981). "Essentials for discrete crack analysis." *Colloquium on Advanced Mechanics of Reinforced Concrete*, IABSE, Zurich, Switzerland, 509–520.
- Colotti, V. (2001). "Modeling of flexural and shear response in reinforced masonry walls under seismic loading." *Masonry Soc. J.*, 19(1), 37–48.
- DIN (Deutsches Institut für Normung). (2007). "Methods of test for masonry. 3: Determination of initial shear strength." *DIN EN1052-3*, Berlin.
- Drysdale, R., Hamid, A., and Baker, L. (1994). *Masonry structures behavior and design*, Prentice Hall, Eaglewood Cliffs, NJ.
- Dulacska, H. (1972). "Dowel action of reinforcement crossing cracks in concrete." *ACI J.*, 69(12), 754–757.
- Hillerborg, A. (1983). "Concrete fracture energy tests performed by 9 laboratories according to a draft RILEM recommendation." Lund Univ., Lund, Sweden.
- Hillerborg, A. (1984). "Numerical methods to simulate softening and fracture of concrete." *Fracture mechanics of concrete*, Martinus Nijhoff Publishers, Leiden, Netherlands.
- ICC (International Code Council). (2009). *2009 international building code*, Country Club Hills, IL.
- Lotfi, H., and Shing, B. (1991). "Appraisal of smeared-crack models for masonry shear wall analysis." *Comput. Struct.*, 41(3), 413–425.
- Lotfi, H., and Shing, B. (1994). "Interface model applied to fracture of masonry structures." *J. Struct. Eng.*, 10.1061/(ASCE)0733-9445(1994)120:1(63), 63–80.
- Lourenco, P. B. (1996). "Computational strategies for masonry structures." Ph.D. dissertation, Delft Univ., Delft, Netherlands.
- Mehrabi, A., Shing, B., Schuller, M., and Noland, J. (1994). "Performance of masonry infilled RC frames under in-plane lateral loads." *Structural engineering and structural mechanics research series*, Univ. of Colorado at Boulder, Boulder, CO.
- Minaie, E. (2009). "Behavior and vulnerability of reinforced masonry shear walls." Ph.D. dissertation, Drexel Univ., Philadelphia.
- NCMA (National Concrete Masonry Association). (2004). "Allowable stress design of concrete masonry." *TEK 14-7A*, Herndon, VA.
- Ngo, D., and Scordelis, A. C. (1967). "Finite element analysis of reinforced concrete beams." *J. Am. Concr. Inst.*, 64(14), 152–163.
- Nilson, A. H. (1968). "Nonlinear analysis of reinforced concrete by the finite element method." *J. Am. Concr. Inst.*, 65(9), 757–766.
- Paulay, T., Park, R., and Phillips, M. (1974). "Horizontal construction joints in cast-in-place reinforced concrete." *ACI J.*, 42, 599–616.
- Rashid, Y. (1968). "Ultimate strength analysis of prestressed concrete pressure vessels." *Nucl. Eng. Des.*, 7(4), 334–344.
- Redmond, L., Ezzatfar, P., DesRoches, R., Stavridis, A., Ozcebe, G., and Kurc, O. (2016a). "Finite element modeling of a reinforced concrete frame with masonry infill and mesh reinforced mortar subjected to earthquake loading." *Earthquake Spectra*, 32(1), 393–414.
- Redmond, L., Kahn, L., and DesRoches, R. (2016b). "Design and construction of hybrid concrete-masonry structures informed by cyclic tests." *Earthquake Spectra*, 32(4), 2337–2355.
- Sayah, A., Stavridis, A., Sherman, J., and McLean, D. (2013). "Finite element modeling of reinforced masonry shear walls under seismic loads." *12th Canadian Masonry Symp.*, Canada Masonry Design Center, Ontario, Canada.
- Sayed-Ahmed, E., and Shrive, N. (1996). "Design of face-shell bedded hollow masonry subject to concentrated loads." *Can. J. Civil Eng.*, 23(1), 98–106.
- Soroushian, P., Obaseki, K., Rojas, M., and Sim, J. (1986). "Analysis of dowel bars acting against concrete core." *ACI J.*, 83(4), 642–649.
- Stavridis, A., and Shing, B. (2010). "Finite-element modeling of nonlinear behavior of masonry-infilled RC frames." *J. Struct. Eng.*, 10.1061/(ASCE)ST.1943-541X.116, 285–296.
- Suidan, M., and Schnobrich, W. (1973). "Finite element analysis of reinforced concrete." *J. Struct. Div.*, 99(10), 2109–2122.
- Wu, Y., Lan, T., Xiao, Y., and Yang, Y. (2016). "Macro modeling of reinforced concrete structural walls: State-of-the-art." *J. Earthquake Eng.*, 1–27.